

Article

# Low Vanadium Permeability Membranes Based on Flexible Hydrophilic Side Chain Grafted Polybenzimidazole/Polymeric Ionic Liquid for VRFBs

Xiaorui Wang<sup>1</sup>, Shuang Wang<sup>1,2,\*</sup>, Dan Liang<sup>1</sup>, Yinghe Cui<sup>1</sup>, Xiaodong Wang<sup>1</sup>, Zhipeng Yong<sup>1</sup>, Fengxiang Liu<sup>1</sup>  
and Zhe Wang<sup>1,2,\*</sup>

<sup>1</sup> School of Chemical Engineering, Changchun University of Technology, Changchun 130012, China

<sup>2</sup> Advanced Institute of Materials Science, Changchun University of Technology, Changchun 130012, China

\* Correspondence: wangshuang@ccut.edu.cn (S.W.); wzccut@126.com (Z.W.)

**Abstract:** Based on amino polybenzimidazoles with flexible hydrophilic side chains (AmPBI-MOE) and polymeric ionic liquid (PIL), a series of composite membranes (AmPBI-MOE-PIL-X) were fabricated for vanadium redox flow battery applications. Here, 1-Bromo-2-(2-methoxyethoxy)ethane was grafted onto amino polybenzimidazole (AmPBI) by the method of halogenated hydrocarbons, and PIL was synthesized from ionic liquids by in situ radical polymerization to build a hydrogen-bonded cross-linked network within the film. The hydrophilic side chain improves the proton conductivity. With the increase in ionic liquids, the vanadium transmittance and the proton conductivity increase. The AmPBI-MOE-PIL-5 membrane not only exhibits a vanadium ions permeability of  $0.88 \times 10^{-9} \text{ cm}^2 \text{ min}^{-1}$ , which is much lower than Nafion117 ( $6.07 \times 10^{-8} \text{ cm}^2 \text{ min}^{-1}$ ), but also shows a very excellent blocking ability for vanadium ion. The AmPBI-MOE-PIL-5 membrane shows excellent performances at  $60 \text{ mA cm}^{-2}$ , with VE of 87.93% and EE of 82.87%, both higher than that of Nafion117 membrane in VRFB.

**Keywords:** low vanadium transmittance; flexible hydrophilic side chains; amino polybenzimidazoles; double-bonded ionic liquid



**Citation:** Wang, X.; Wang, S.; Liang, D.; Cui, Y.; Wang, X.; Yong, Z.; Liu, F.; Wang, Z. Low Vanadium Permeability Membranes Based on Flexible Hydrophilic Side Chain Grafted Polybenzimidazole/Polymeric Ionic Liquid for VRFBs. *Batteries* **2023**, *9*, 141. <https://doi.org/10.3390/batteries9020141>

Academic Editor: Ki Jae Kim

Received: 27 December 2022

Revised: 31 January 2023

Accepted: 17 February 2023

Published: 20 February 2023



**Copyright:** © 2023 by the authors. Licensee MDPI, Basel, Switzerland. This article is an open access article distributed under the terms and conditions of the Creative Commons Attribution (CC BY) license (<https://creativecommons.org/licenses/by/4.0/>).

## 1. Introduction

With environmental pollution and the increasing reduction in energy, the development of sustainable energy, green energy and renewable energy has become the research focus of the world. Vanadium redox flow batteries (VRFBs), one of the large-scale energy storage systems, utilize changes in the valence state of vanadium ions to realize a mutual conversion of electrical energy and chemical energy [1–3]. It has attracted widespread attention owing to its advantages, for example, flexible design, high efficiency, safety, low impact on the environment and the ability to integrate intermittent power generation into the grid [4–6]. It is believed that it will achieve large-scale promotion and application in the future, and is regarded as one of the most promising new energy-supporting energy storage technologies. One of the characteristics of VRFB is an oxidation-reduction battery with vanadium as the only active material in a circulating liquid state. The vanadium ion has four different valence states in sulfuric acid solution. This helps to rebalance and reuse the battery [7,8]. Since cross contamination of electrolytes is usually the biggest problem causing capacity loss, based on the application of VRFB the initial capacity can be restored by mixing and refilling anode electrolyte and cathode electrolyte [9–11]. In addition, the reuse of electrolytes can reduce the cost of system operation. For VRFB, electrodes, electrolytes, and membranes have a significant impact on battery performance. Researchers have never stopped optimizing VRFB technology, such as nano-fluid electrolyte technology, electrolyte rebalancing methods, electrode oxidation activation method and modified membrane, etc. [12–15]. For batteries, the ion exchange film is a significant constituent, and it provided

the ion transport channel, realizes the construction of a complete circuit in battery structure by selectively penetrating ions, and prevents vanadium ion infiltration and mixing in the positive and negative electrodes [16–18]. The properties of the film, in significant measure, determine the performance of the battery. The ideal membrane needs to have the following characteristics: low vanadium ion permeability, reducing the pollution caused by vanadium ion transmembrane transport; excellent chemical stability and high mechanical strength making the membrane have a long service life under acidic conditions, thus increasing the battery life; and high ionic conductivity and good ionic selectivity make the battery efficient. The low processing and production cost is conducive to the wide application of diaphragm [5,6,16–19].

The proton exchange membrane, represented by the Nafion membrane produced by DuPont, is widely used in the commercial field. Its sulfonic acid group is used as the exchange group as the standard membrane of the vanadium redox flow battery. The Nafion membranes have excellent battery performance, high stability in the electrolyte, high mechanical strength, and high conductivity. However, due to the defects of high vanadium ion permeability and high price, this also limits the further development of the flow battery to a certain extent [16,19,20]. There are many ways to reduce vanadium permeability, such as polymer blending, surface modification, nanoparticle addition, monomer grafting, etc. [7,8,19,21]. These methods effectively reduce vanadium permeability, but the high cost hinders their application in VRFBs. Finding alternatives to Nafion membranes has become a research hotspot.

Polybenzimidazole (PBI) was first introduced as a proton exchange membrane for VRFBs applications in 2015 [22]. PBI is an aromatic heterocyclic polymer containing imidazole groups [23–27]. The dense structure of PBI can reduce the permeability of  $\text{VO}^{2+}$  ions, and PBI with excellent chemical durability, high mechanical properties, and little cost has brought about widespread attention in the practical application of VRFBs [28–33]. Nevertheless, the area resistance of the original PBI is large. For the purpose of shortening the area resistance of PBI, a lot of efforts have been made by many researchers, such as adding ionic groups [34,35]. Ding et al. introduced sulfonic acid groups into PBI, and the area resistance of SPBI-30 reduced from 0.45 to 0.3  $\Omega \text{ cm}^2$ , but the vanadium transmittance rose [34]. In addition, adding ionic liquid is also an effective way [36,37]. Song and his co-workers added the [BMIm]BF<sub>4</sub> ionic liquid to the polymer, and with [BMIm]BF<sub>4</sub> added it is a gradual decrease in area resistance of the composite membrane, indicating that the ILs could enhance the proton transport capability of OPBI/BF<sub>4</sub>-X membranes [36]. Therefore, it is important to reduce the vanadium permeability while reducing the area resistance. Adding inorganic filler or introducing porous structures can effectively improve this situation [9,38–40]. Liang et al. prepared SPBI and mixed the UiO-66 with the polymer, forming the denser network structure that acts as a barrier to prevent  $\text{VO}^{2+}$  ions from penetrating, while reducing the area resistance [39]. In addition, introducing side-chain structures into the PBI matrix is also a good method [10,11,23,41]. Ren et al. synthesized a range of quaternary ammonium groups grafted PBI membranes, which improved the free volume and hydrophilicity of films and resulted in lower area resistance. Meanwhile, when the DG% increased from 0% to 9%, the vanadium transmittance of PBI-x%EPTMA reduced from  $2.0 \times 10^{-7}$  to  $1.0 \times 10^{-7} \text{ cm}^2 \text{ min}^{-1}$  [23]. However, for grafting side chains on the membrane, if the side chains contain ionic groups, ionic groups will reduce the chemical durability, while non-ionic side chains can effectively avoid the above situation. The non-ionic oxygen-containing hydrophilic side chains have flexibility and high hydrophilic properties, which can increase the free volume and hydrophilic properties of the polymer [11,17]. Until now, the optimization of the area resistance, and  $\text{VO}^{2+}$  permeability has been the top-drawer critical factor in the development of proton exchange membranes for VRFB applications.

In this work, grafting 1-Bromo-2-(2-methoxyethoxy) ethane synthesized AmPBI-MOE. By choosing the appropriate degree of grafting, vanadium ion permeation can be effectively avoided. The membrane with the grafting degree of 20% has the best vanadium resistance,

and the vanadium permeability is only  $8.8 \times 10^{-10} \text{ cm}^2 \text{ min}^{-1}$ . The AmPBI synthesized by our group has a quantitatively controllable 5-aminoisophthalic acid content, and can reduce the -NH- site on imidazole occupied by grafting as well. The optimal ratio of amino groups on the main chain of AmPBI was determined by proton conductivity value. Meanwhile, the polymeric ionic liquid was introduced into the system to build a hydrogen bond cross-linked network, which further improved the proton conductivity and enabled the AmPBI-MOE-PIL membrane to obtain excellent performance.

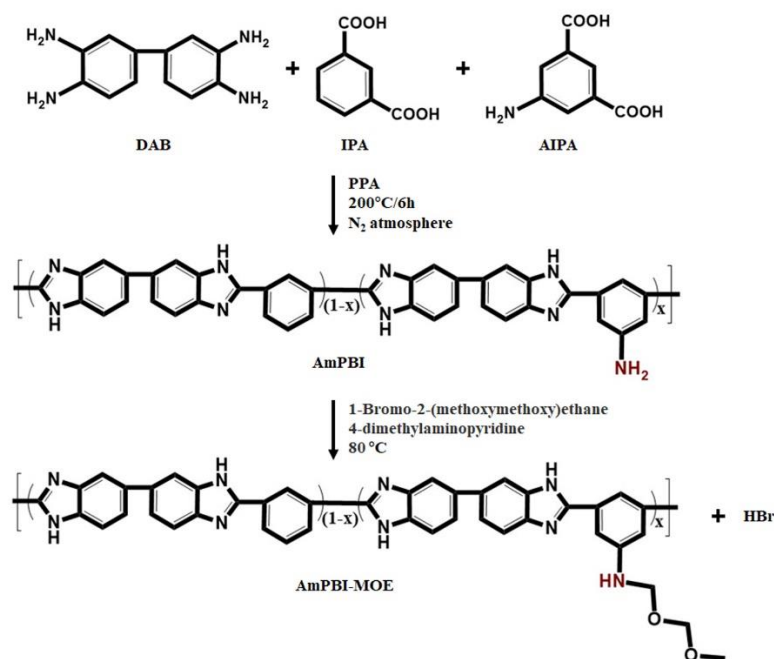
## 2. Experimental

### 2.1. Materials

Isophthalic acid (IPA), polyphosphoric acid (PPA), phosphorus pentoxide ( $\text{P}_2\text{O}_5$ ), 5-aminoisophthalic acid (AIPA), 1-Bromo-2-(2-methoxyethoxy) ethane, 3,3',4,4'-diaminobenzidine (DAB), 4-Dimethylaminopyridine (DMAP) and Vanadium(IV) sulfate oxide hydrate were purchased from Macklin. Dimethyl sulfoxide (DMSO), 2,2'-Azobis(2-methylpropionitrile) (AIBN), triethylamine, and acetone were procured from Aladdin.

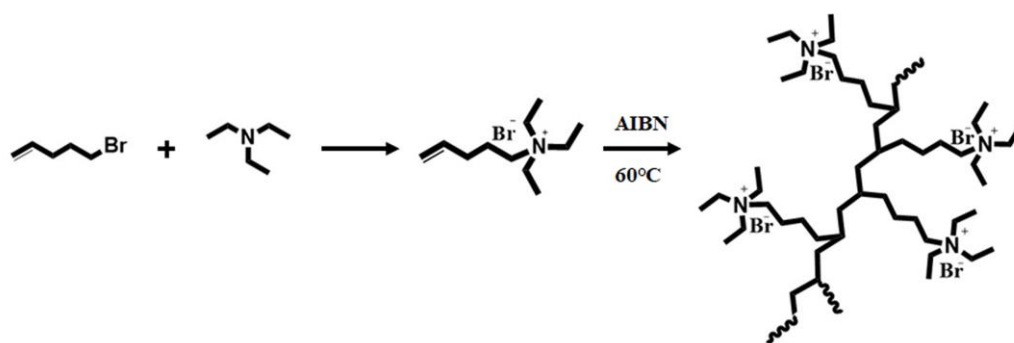
### 2.2. Preparation of the AmPBI and Ionic Liquids

As shown in Scheme 1, the AmPBI was prepared by the conventional method [42]. Firstly, PPA was placed into a four-necked flask and stirred at  $130 \text{ }^\circ\text{C}$  for 1.5 h, and then DAB, IPA,  $\text{P}_2\text{O}_5$ , and AIPA were soaked in the four-necked flask and stirred at  $130 \text{ }^\circ\text{C}$  for 5 h. Following this, the reaction was slowly heated to  $210 \text{ }^\circ\text{C}$  for 5–6 h. The fully reactive solution was placed into water, then the product was neutralized with an ammonia solution. After drying by drying in an oven, AmPBI was obtained. The optimal molar ratio of IPA and AIPA determined by the proton conductivity test is 0.8:0.2, as shown in Figure S1. Tested by the Ubbelohde viscometer, the inherent viscosity of AmPBI is 0.64. The molecular weight of AmPBI was 27150.



**Scheme 1.** Synthesis process of AmPBI-MOE.

The preparation of ionic liquids (IL) was accomplished by a typical reaction [43]. The mixture of triethylamine and 5-Bromo-1-pentene was heated by condensation at  $75 \text{ }^\circ\text{C}$  for 48 h under mechanical rabbling. The mixture was washed with acetone several times and removed by vacuum distillation to obtain the target product, the white solid powder. The synthesis process of PIL is shown in Scheme 2.



**Scheme 2.** Synthesis process of PIL.

### 2.3. Synthesis of the AmPBI-MOE

AmPBI was dispersed in Dimethyl sulfoxide with magnetic stirring. After the solution is fully dispersed, DMAP and 1-Bromo-2-(2-methoxyethoxy) ethane were mixed in this reaction mixture and reacted with magnetic stirring at 90 °C for one day. After washing with acetone, the brown precipitate was obtained. The AmPBI-MOE was obtained (the degree of graft (DG) = 5%, 10%, 20%, 30%). The synthesis process is as in Scheme 1. By comparing the vanadium transmittance, the optimal DG is 20%, as shown in Figure S2.

### 2.4. Preparation of AmPBI-MOE-PIL-X Composite Membranes

AmPBI-MOE-PIL-X were prepared by solution casting method. AmPBI-MOE and IL were dispersed in DMSO together. At the same time, 1 wt.% of AIBN was added to the mixture as the initiator. The mixture was filtered onto a glass plate (10 × 10 cm<sup>2</sup>), set at a vacuum oven temperature to 55 °C for 3 h, and then 90 °C for 18 h; the AmPBI-MOE-PIL-X composite membranes were then prepared.

### 2.5. Characterization and Measurements

#### 2.5.1. Structural Characterizations

The Fourier transform infrared (FT-IR) spectra of the films and IL were obtained using a Vector-22 spectrometer (Bruker, Germany) in a range of 4000 cm<sup>-1</sup> to 400 cm<sup>-1</sup>. The IL, AmPBI, and AmPBI-MOE were characterized by <sup>1</sup>H-NMR spectra with Bruker AVANCE III 400 MHz spectrometer.

#### 2.5.2. Scanning Electron Microscopy

The microscopic morphology of the cross-section of the film was characterized by scanning electron microscope with JSM-7610FPlus. This cross-section of the film was obtained by embrittlement of membranes in liquid nitrogen.

#### 2.5.3. Water Uptake, Swelling Ratio, and Ion Exchange Capacity

The anions in AmPBI-MOE-PIL-X membranes were converted to OH<sup>-</sup> by soaking in KOH solution for 20 h. The resulting films were immersed in the 3 M H<sub>2</sub>SO<sub>4</sub>. The IEC was measured by the inverse titration method. Firstly, the film was soaked in the 3 M H<sub>2</sub>SO<sub>4</sub> and placed in 1 M NaCl aqueous solutions for 48 h. After dropping a drop of phenolphthalein, the solution was inversely titrated with a 0.01 M NaOH solution. The WU, SR, and IEC of membranes are computed with Equations (1)–(3):

$$\text{WU}(\%) = \frac{m_{\text{wet}} - m_{\text{dry}}}{m_{\text{dry}}} \times 100\% \quad (1)$$

$$\text{SR}(\%) = \frac{V_{\text{wet}} - V_{\text{dry}}}{V_{\text{dry}}} \times 100\% \quad (2)$$

$$\text{IEC} = \frac{C_{\text{NaOH}} V_{\text{NaOH}}}{m_{\text{dry}}} \times 100\% \quad (3)$$

where,  $m_{\text{wet}}$ ,  $V_{\text{wet}}$  are the weight and volume of the water-saturated film,  $m_{\text{dry}}$  and  $V_{\text{dry}}$  are the weight and volume of the dried film.

#### 2.5.4. Vanadium Permeability

The less vanadium exudation, the better the effect on the performance of vanadium redox flow batteries. The Permeability of  $\text{VO}^{2+}$  was measured by an H-shaped diffusion battery. The left and right diffusion cells were filled with 1.5 M  $\text{MgSO}_4/3$  M  $\text{H}_2\text{SO}_4$  and 1.5 M  $\text{VOSO}_4/3$  M  $\text{H}_2\text{SO}_4$ , separately. Take out 4 mL of solution from the diffusion cell on the right side at the specified time to measure the vanadium ions concentration in the  $\text{MgSO}_4$  solution. The concentration of vanadium ions was monitored on a UV-Vis spectrometer, and the permeability of  $\text{VO}^{2+}$  was determined with the Equation below:

$$P = \frac{L \cdot V_b}{A \cdot C_a} \left( \frac{d(C_b(t))}{dt} \right) \quad (4)$$

where  $A$  represents the effective area and  $L$  is the thickness of the film.  $V_b$  represents the volume of  $\text{MgSO}_4$  solution,  $C_a$  and  $C_b(t)$  are the vanadium ions concentration in  $\text{VOSO}_4$  solution and vanadium ions concentration in  $\text{MgSO}_4$  solution, separately.  $P$  represents vanadium ions permeability.

#### 2.5.5. Area Resistance

Under electrochemical impedance method spectroscopy (EIS), the area resistance (AR) of membranes was measured. The electrochemical workstation operates at a frequency of 100 kHz to 100 Hz. The AR was computed shown as Equation (5):

$$\text{AR} = S(R_1 - R_2) \quad (5)$$

where  $R_1$  and  $R_2$  are the resistance of the battery with and without a film in the clamp, separate.  $S$  represents the effective area ( $9 \text{ cm}^2$ ).

#### 2.5.6. Chemical Stability

Put to use the 0.1 mol/L  $\text{VO}^{2+} + 3.0$  mol/L  $\text{H}_2\text{SO}_4$  acid  $\text{VO}_2^+$  solution to study the oxidation stability of the film. The films were completely immersed in an acid  $\text{VO}_2^+$  solution. After 28 days the morphology of the membrane was observed and FTIR data were obtained.

#### 2.5.7. VRFB Cell Performance

The battery performance was estimated by the electrochemical workstation (LANHE CT3001A) at room temperature at the permanent current density of  $40 \text{ mA cm}^{-2}$  to  $120 \text{ mA cm}^{-2}$ . The battery was constructed by sandwiching a film between graphite felts. The effective area was  $9 \text{ cm}^2$ . In addition, this cut-off voltage was set as 0.9 and 1.55 V. 1.5 M  $\text{V}^{3+}/3$  M  $\text{H}_2\text{SO}_4$  and 1.5 M  $\text{VO}_2^+/3$  M  $\text{H}_2\text{SO}_4$  solution were used as cathode and anode electrolytes. Before battery performance testing, soak the membrane in 3 M  $\text{H}_2\text{SO}_4$  solution at  $40^\circ \text{C}$  for 24 h. Calculate the efficiency of the charge-discharge cycle by the Equations (6)–(8):

$$\text{CE}(\%) = \frac{\int I_d dt}{\int I_c dt} \times 100\% \quad (6)$$

$$\text{VE}(\%) = \frac{\text{EE}}{\text{CE}} \times 100\% \quad (7)$$

$$\text{EE}(\%) = \frac{\int V_d I_d dt}{\int V_c I_c dt} \times 100\% \quad (8)$$

where  $I$  is current,  $V$  and  $t$  are voltage and time in sequence,  $d$  and  $c$  are discharge and charge process, separately.

### 2.5.8. Proton Conductivity

The proton conductivity of membranes was determined by the four-electrode method on Metrohm Autolab PGSTA T302N. Prior to testing, the membrane was sequentially immersed in 3 M sulfuric acid for 24 h and deionized water for 24 h at 40 °C. The proton conductivity ( $\sigma$ ) is computed shown as Equation (9):

$$\sigma = \frac{L}{A \times R} \quad (9)$$

where  $A$  is cross-sectional area of the membranes, and  $L$  is distance between two electrodes.

### 2.5.9. Ion selectivity

Ion selectivity is also an important basis for judging the excellent performance of membrane materials for batteries. The following equation could be used to calculate the ion selectivity.

## 3. Results and Discussion

### 3.1. Synthesis and Characterization

The preparation of ionic liquids (IL) was accomplished by the typical reaction. Figure 1a shows the  $^1\text{H-NMR}$  spectra of [TPAm]Br and all the film. The peaks on IL (a' b' c') correspond to 4.88, 3.22, 1.25 ppm, respectively, which were consistent with literature reports [42–44]. The double-bonded groups in IL form a cross-linked network by radical polymerization [43]. The absorption peak of imidazole-NH at 13.2 ppm proved the synthesis of AmPBI [42,45]. In addition, the primary amine group in the range of 5.4–6 ppm for AmPBI can be seen. However, the primary amine group disappeared after grafting and the secondary ammonia group appeared near 7 ppm. As a result, AmPBI and AmPBI-MOE-PIL-X were successfully synthesized.

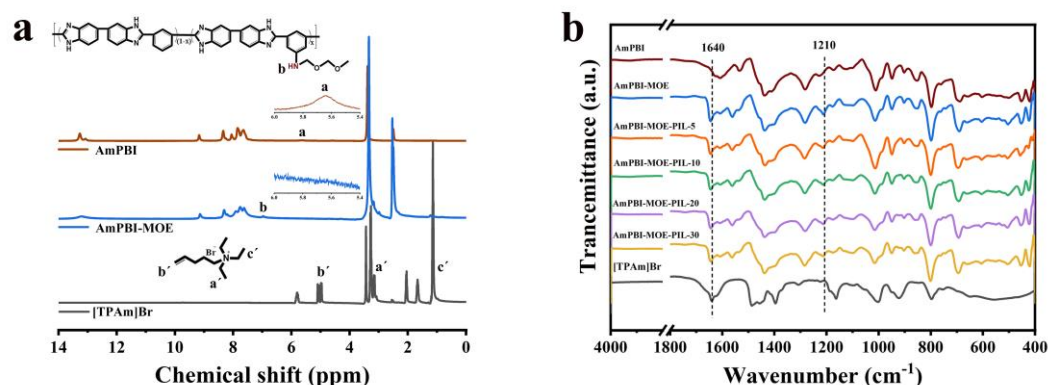


**Figure 1.**  $^1\text{H-NMR}$  spectra (a) of [TPAm]Br, AmPBI, and AmPBI-MOE; FTIR spectra (b) of [TPAm]Br and all the membranes.

FTIR spectroscopy further characterized the chemical structures of IL and all the membranes, as shown in Figure 1b. After grafting, the absorption peak at  $1210\text{ cm}^{-1}$  was  $-\text{C}-\text{O}-\text{C}-$  bond stretching vibration, indicating that the grafting was successful [11]. In the meantime,  $1640\text{ cm}^{-1}$  was the stretching vibration of the  $\text{C}=\text{C}$  bond [43,44]. Characteristic peaks of the double bonds group in IL disappeared in the membranes, which proves that the cross-linked networks were formed by the polymerization of free radical in the process of membranes preparation.

### 3.2. Microscopic Morphology

The internal microstructures of all the films can be studied from the cross-section SEM photographs in Figure 2. There are some squamous structures on the membrane cross-section surface due to plastic deformation during brittle fracture [42,44,45]. The microstructure of the membranes did not change obviously after grafting side chains. It can be clearly observed that the plastic deformation of the AmPBI-MOE-PIL-20 and 30 membranes are continuously reduced, and the toughness of the membranes is enhanced due to the incorporation of PIL. Moreover, all the membranes are compact, which means that the incorporation of PIL into the polymer matrix will not cause defects within the polymer.

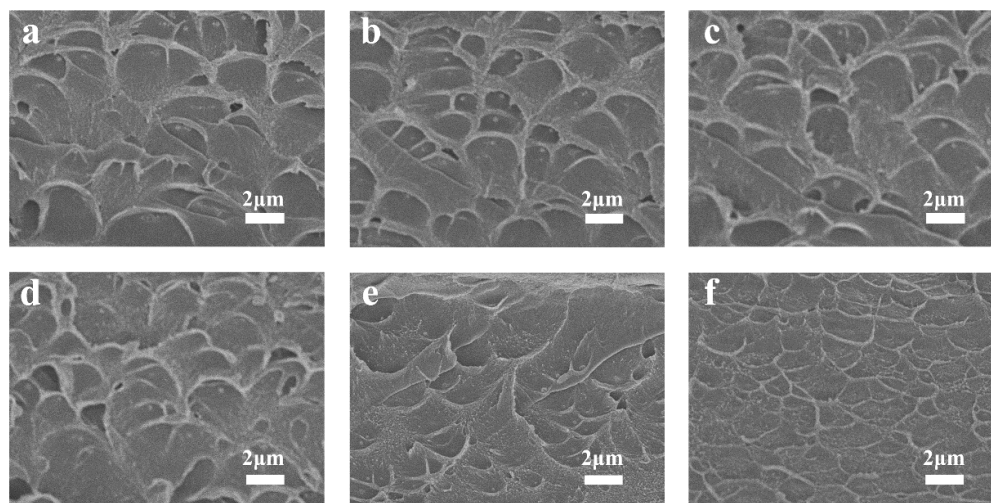


**Figure 2.** The cross-section SEM of AmPBI and AmPBI-MOE-PIL-X (X = 0%, 5%, 10%, 20%, 30%) membranes (a–f).

### 3.3. Physicochemical Properties of Membranes

The Water uptake (WU), Swelling ratio (SR), and Ion exchange capacity (IEC) are shown in Table 1. Water uptake after grafting is increased due to the hydrophilic side chain and larger free volume. PIL added to the polymer produces a crosslinking structure, and the free volume within the polymer is filled by the cross-linking network architecture of the PIL, thus inhibiting the water uptake and ion exchange capacity as PIL increases from 5% to 30% [36,44]. The main factor affecting the SR of the films is the framework structure of the polymer. The modified film showed a similar SR tendency as the AmPBI membrane, verifying that the incorporation of PIL did not change the internal structure of the membrane [36,37]. With the addition of PIL from 5% to 30%, the conductivity increased from 7.9 to 9.5 mS cm<sup>-1</sup>. The introduction of PIL increases the free volume and the PIL itself acts as a transport carrier, both of which improve the proton conductivity simultaneously [44]. The VO<sup>2+</sup> permeability reduced from 3.25 × 10<sup>-9</sup> to 0.85 × 10<sup>-9</sup> cm<sup>2</sup> min<sup>-1</sup> after grafting, which greatly improves the ability to block the VO<sup>2+</sup> transport. All thickness was measured more than three times with a micrometer to reduce errors.

**Table 1.** Water uptake, proton conductivity, ion exchange capacity, swelling ratio and VO<sup>2+</sup> permeability of AmPBI, AmPBI-MOE-PIL-X membranes, and Nafion117.

Samples	Thickness (μm)	Water Uptake (%)	Swelling Ratio (%)	IEC (mmol g <sup>-1</sup> )	Proton Conductivity (mS cm <sup>-1</sup> )	VO <sup>2+</sup> Permeability (10 <sup>-9</sup> cm <sup>2</sup> min <sup>-1</sup> )
AmPBI	35	24.3 ± 0.5	13.2 ± 1.0	0.42	7.9	3.25
AmPBI-MOE	37	26.5 ± 0.3	14.9 ± 0.7	0.41	8.1	0.85
AmPBI-MOE-PIL-5	36	27.7 ± 0.6	14.0 ± 0.4	0.47	8.5	0.88
AmPBI-MOE-PIL-10	30	24.1 ± 0.4	14.1 ± 0.3	0.48	8.8	0.93
AmPBI-MOE-PIL-20	34	15.4 ± 0.5	13.8 ± 0.7	0.39	9.4	0.98
AmPBI-MOE-PIL-30	27	12.9 ± 0.5	14.4 ± 0.8	0.37	9.5	0.99
Nafion117	180	22.7 ± 0.5	43.8 ± 1.2	1.10	49.2	60.67

### 3.4. Vanadium Permeability, Ion Selectivity, and Area Resistance

VRFB self-discharge can be induced by the transmembrane movement of vanadium ions [20]. Therefore, the excellent ability to block vanadium ion transport is the key to the membrane. Compared with Nafion117, a series of AmPBI membranes exhibited lower vanadium permeability, on account of the dense structure of AmPBI and other composite membranes in Figure 3a [28–30]. By grafting side chains, a significant reduction in vanadium permeability can be seen. This is a result of the addition of flexible side chains, which efficiently reduce the transmission of larger vanadium ions [10,11,23,41]. By comparing the vanadium transmittance, DG = 20% is the best, as shown in Figure S2. With the increase in ionic liquid there is a negative effect on vanadium blocking effect. It is found that the  $\text{VO}^{2+}$  permeability of the AmPBI-MOE-PIL-5 was  $0.88 \times 10^{-9} \text{ cm}^2 \text{ min}^{-1}$ , which was much lower than that of Nafion117 ( $60.67 \times 10^{-9} \text{ cm}^2 \text{ min}^{-1}$ ). Then the ion selectivity of AmPBI-MOE-PIL-5 is much higher than that of Nafion117.

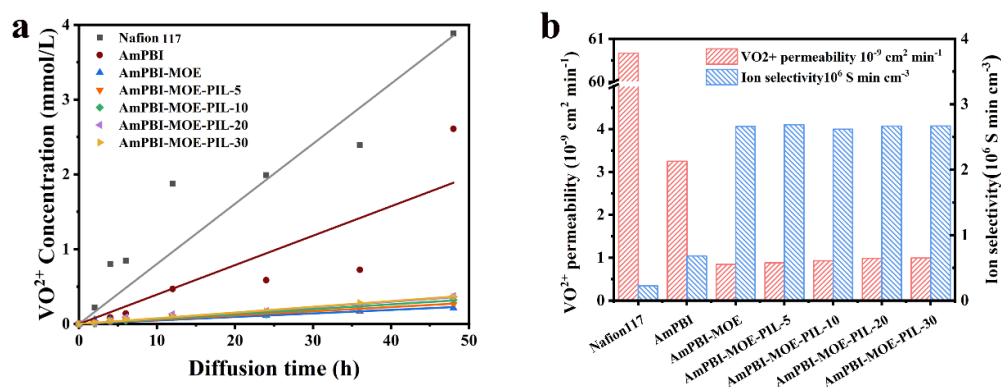


**Figure 3.** Vanadium concentration curve (a) and ion selectivity (b) of AmPBI, AmPBI-MOE-PIL-X membranes, and Nafion117.

The area resistance (AR) is another key parameter for judging the membrane performance [45–48]. Figure 4 shows the AR of the AmPBI and AmPBI-MOE-PIL-X membranes. Due to the larger thickness of Nafion117 film, the AR of Nafion117 was higher than that of other membranes [39,49]. After grafting and adding appropriate PIL, the ARs of the composite membranes decrease. It is found that the AR for AmPBI-MOE-PIL-5 is  $0.7 \Omega \text{ cm}^2$ , which is the lowest. The results proved that grafting hydrophilic side chains and adding an appropriate amount of ionic liquid can effectively curb the area resistance and promote proton conductivity.

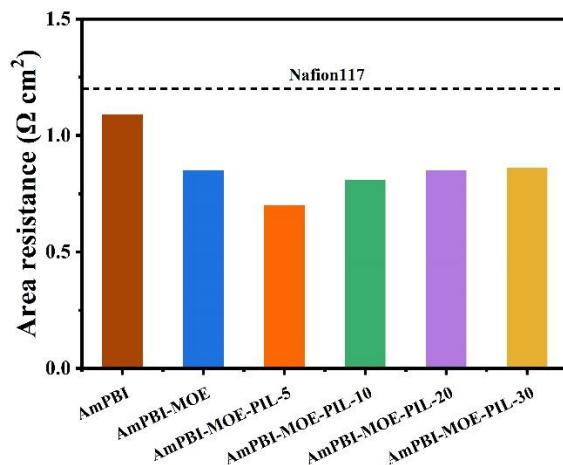


**Figure 4.** The area resistance of AmPBI, AmPBI-MOE-PIL-X membranes, and Nafion117.

### 3.5. Mechanical Properties

During the operation of the battery the membrane needs to withstand the impact of the electrolyte and the extrusion of the graphite felt fiber, so the film must have good mechanical properties. As shown in Figure 5, it is the mechanical properties of all the films. It can be seen that the grafting of oxygen-containing side chains reduces the mechanical strength of the modified membranes [23,41]. This is because the intermolecular interaction forces of the polymeric backbone are reduced after the grafting of side chains [45]. Due to the plasticizing effect of PIL, adding a certain amount of PIL increases the elongation at break [36]. When the mass ratio of PIL was 20% the elongation at the break of the membrane showed a maximum value (18.2%). The elongation at break reduces with enhancement the enhancement of PIL, which is due to the uneven dispersion of excess PIL in the membrane. Hence, the mechanical properties of the films fully meet the requirements of VRFBs.

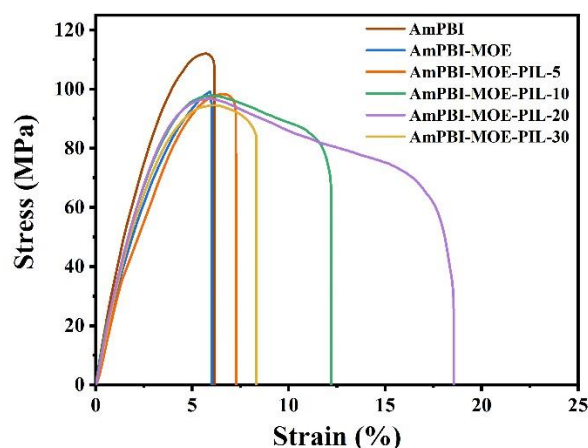
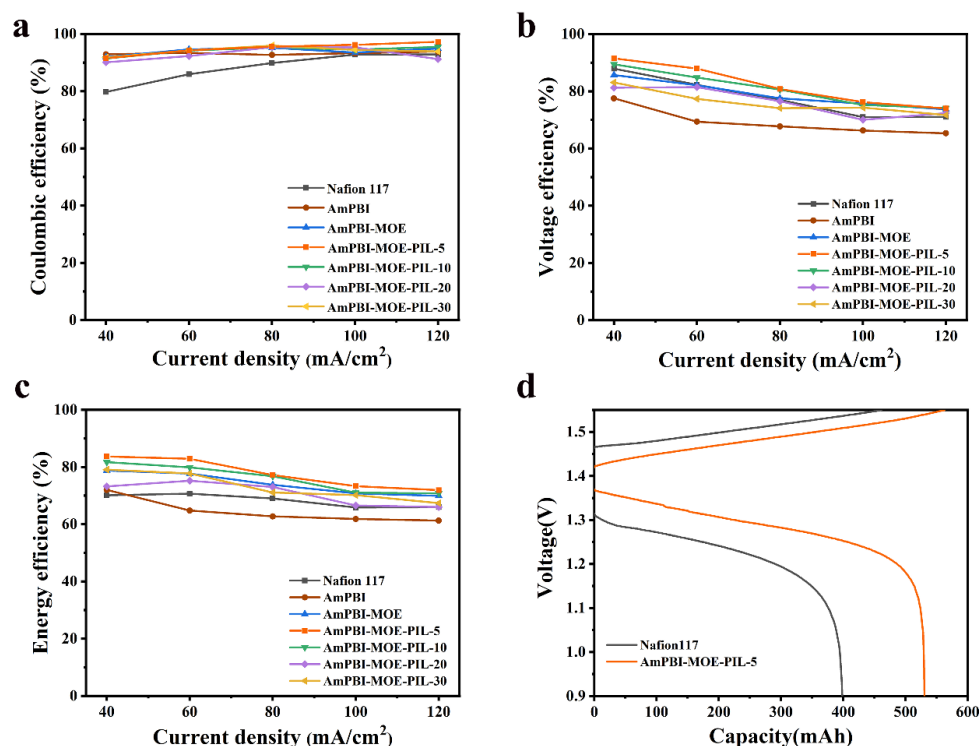


Figure 5. Mechanical properties of AmPBI, AmPBI-MOE-PIL-X membranes.

### 3.6. VRFB Performance

The VRFB performance comparison data of membranes with different PIL addition content and Nafion117 are shown in Figure 6. As shown in Figure 6a, the coulombic efficiencies of a series of films modified with AmPBI as the substrate is all above 90% at current densities ranging from 120 to 40 mA cm<sup>-2</sup>, which is higher than that of Nafion117. This is due to the dense structure of the PBI itself, where its excellent vanadium-blocking ability reduces the self-discharge behavior during the process of charging and discharging [29,30]. In addition, the grafting of hydrophilic flexible side chains further reduces the cross-mixing of vanadium ions as well as improved the proton transport performance. With the addition of grafting and PIL, the area resistance can affect the voltage efficiency, the area resistance further decreases, and the voltage efficiency also shows the same law [22]. Due to over-potential and ohmic polarization, the voltage efficiency of all membranes reduces with augmented current density. Energy efficiencies represent the energy utilization rate of the energy storage system in the charging and discharging process, and are also an important indicator for VRFB [16]. All membranes in Figure 6c have higher energy efficiencies than that of Nafion117. It is shown that the modified membrane has better VRFB performance. The AmPBI-MOE-PIL-5 shows much higher energy efficiencies. Figure 6d represents the charge–discharge curve of the AmPBI-MOE-PIL-5 membrane at 60 mA cm<sup>-2</sup>. The AmPBI-MOE-PIL-5 shows good battery charge–discharge performance. The discharge capacity of the AmPBI-MOE-PIL-5 tested under the same conditions can reach 530 mAh, while that of Nafion117 is 400 mAh. The oxidative stability of the AmPBI-MOE-PIL-5 membranes was evaluated in Figure S3. The oxidative stability of polymer membrane materials will be more concern in future work. As shown in Table 2, the AmPBI-MOE-PIL-5 shows excellent long-term performance at 60 mA cm<sup>-2</sup>.



**Figure 6.** Cell performances (a) CE, (b) VE, (c) EE of AmPBI-MOE-PIL-X and Nafion117 membranes, charge–discharge curve (d) at  $60 \text{ mA} \cdot \text{cm}^{-2}$ .

**Table 2.** Performances of several batteries with various functionalized PBI membranes.

Membrane	Thickness ( $\mu\text{m}$ )	AR ( $\Omega \text{ cm}^2$ )	Current Density ( $\text{mA} \cdot \text{cm}^{-2}$ )	CE (%)	VE (%)	EE (%)
AmPBI-MOE-PIL-5	36	0.70	60	94.3	87.9	82.9
PBI-100 [46]	-	0.70	60	~100	~82	~82
50-SPBI [15]	39	~2.7	60	-	-	~77
PBI [22]	-	-	60	99	74	74
ScABPBI [47]	65	0.34	60	97	85	~82
72P-24S PBI [30]	76	0.43	60	97	85	~84
mPBI [29]	35	2.03	80	~98	~69	~68
PBI-40-SiO <sub>2</sub> [48]	-	~0.28	80	99.5	77	76.8

To further investigate the long-term stability of the composite films, they were subjected to 200 charge–discharge cycles at  $60 \text{ mA cm}^{-2}$ . AmPBI-MOE-PIL-5 still maintained excellent battery performance after 200 cycles of performance test, including CE (93.41%), VE (84.96%), and EE (79.37%) in Figure 7a. The capacitance retention rate is a good indicator of the long-term performance of the cell.

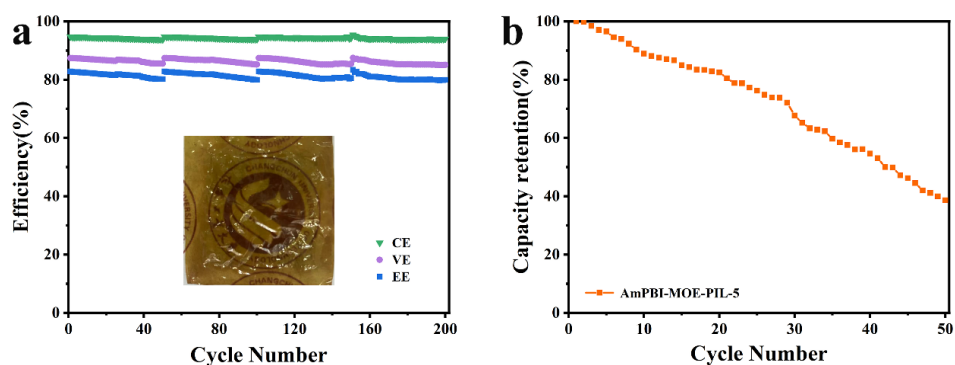


**Figure 7.** Cycling performances of the efficiencies (a), discharge capacity reduction (b) of AmPBI-MOE-PIL-5 at  $60 \text{ mA cm}^{-2}$ .

#### 4. Conclusions

A hydrophilic side-chain AmPBI membrane with low area resistance and low vanadium transmittance was synthesized for VRFB. The AmPBI-MOE-PIL-5 membrane shows a  $\text{VO}^{2+}$  permeability of  $0.88 \times 10^{-9} \text{ cm}^2 \text{ min}^{-1}$ , which is much lower than that of Nafion117 ( $60.67 \times 10^{-9} \text{ cm}^2 \text{ min}^{-1}$ ); it also shows a low AR of  $0.70 \Omega \text{ cm}^2$ , which is much lower than Nafion117 membrane ( $1.19 \Omega \text{ cm}^2$ ). The AmPBI-MOE-PIL-5 showed excellent VRFB performances at  $60 \text{ mA cm}^{-2}$ , with VE of 87.93%, CE of 94.25%, and EE of 82.87%, which are higher than those of Nafion117. Under the same conditions, the discharge capacity of the AmPBI-MOE-PIL-5 can reach 530 mAh, while the Nafion117 is 400 mAh. This work provides a high-performance AmPBI membrane grafted with hydrophilic side chains for VRFB—a promising candidate for VRFB applications.

**Supplementary Materials:** The following supporting information can be downloaded at: <https://www.mdpi.com/article/10.3390/batteries9020141/s1>, Figure S1: Proton conductivity of amino PBI membrane (different amino-modified degree is 0.95:0.05, 0.9:0.1, 0.85:0.15, 0.8:0.2). Figure S2: Vanadium concentration curve of AmPBI-MOE (the degree of graft (DG) = 10 %, 20 %, 30 %, 40 %). Figure S3: The oxidative stability of the AmPBI-MOE-PIL-5 membranes. Figure S4: Thermal stability of composite membranes.

**Author Contributions:** Conceptualization, X.W. (Xiaorui Wang) and S.W.; methodology, X.W. (Xiaorui Wang); software, X.W. (Xiaorui Wang); validation, X.W. (Xiaorui Wang); formal analysis, X.W. (Xiaorui Wang), D.L., Z.Y. and X.W. (Xiaodong Wang); investigation, X.W. (Xiaorui Wang), F.L. and Y.C.; resources, S.W. and Z.W.; data curation, X.W. (Xiaorui Wang); writing—original draft preparation, X.W. (Xiaorui Wang); writing—review and editing, X.W. (Xiaorui Wang) and S.W.; visualization, X.W. (Xiaorui Wang); supervision, S.W. and Z.W.; project administration, S.W.; funding acquisition, S.W. All authors have read and agreed to the published version of the manuscript.

**Funding:** The authors gratefully acknowledge the financial support of this work by Department of Science and Technology of Jilin Province (YDZJ202201ZYTS570), Education Department of Jilin Province (Grant no. JJKH20220669KJ), Open Project of State Key Laboratory of Supramolecular Structure and Materials (sklssm2022018), Department of Science and Technology of Jilin Province (grant no. 20180101209JC), Natural Science Foundation of China (grant no. 22075031).

**Institutional Review Board Statement:** Not applicable.

**Informed Consent Statement:** Not applicable.

**Conflicts of Interest:** The authors declare no conflict of interest.

#### References

1. Jung, J.; Won, J.; Hwang, S.S. Highly selective composite membranes using ladder-like structured polysilsesquioxane for a non-aqueous redox flow battery. *J. Membr. Sci.* **2020**, *595*, 117520. [CrossRef]
2. Shi, M.; Dai, Q.; Li, F.; Li, T.; Hou, G.; Zhang, H.; Li, X. Membranes with Well-Defined Selective Layer Regulated by Controlled Solvent Diffusion for High Power Density Flow Battery. *Adv. Energy Mater.* **2020**, *10*, 2001382. [CrossRef]
3. Zhao, Y.; Li, M.; Yuan, Z.; Li, X.; Zhang, H.; Vankelecom, I.F.J. Advanced Charged Sponge-Like Membrane with Ultrahigh Stability and Selectivity for Vanadium Flow Batteries. *Adv. Funct. Mater.* **2016**, *26*, 210–218. [CrossRef]
4. Geng, K.; Li, Y.; Xing, Y.; Wang, L.; Li, N. A novel polybenzimidazole membrane containing bulky naphthalene group for vanadium flow battery. *J. Membr. Sci.* **2019**, *586*, 231–239. [CrossRef]
5. Jia, C.; Liu, J.; Yan, C. A significantly improved membrane for vanadium redox flow battery. *J. Power Sources* **2010**, *195*, 4380–4383. [CrossRef]
6. Mu, D.; Yu, L.; Liu, L.; Xi, J. Rice Paper Reinforced Sulfonated Poly(ether ether ketone) as Low-Cost Membrane for Vanadium Flow Batteries. *ACS Sustain. Chem. Eng.* **2017**, *5*, 2437–2444. [CrossRef]
7. Xu, W.; Long, J.; Liu, J.; Luo, H.; Duan, H.; Zhang, Y.; Li, J.; Qi, X.; Chu, L. A novel porous polyimide membrane with ultrahigh chemical stability for application in vanadium redox flow battery. *Chem. Eng. J.* **2022**, *428*, 131203. [CrossRef]
8. Escorihuela, J.; Sahuquillo, O.; Garcia-Bernabe, A.; Gimenez, E.; Compan, V. Phosphoric Acid Doped Polybenzimidazole (PBI)/Zeolitic Imidazolate Framework Composite Membranes with Significantly Enhanced Proton Conductivity under Low Humidity Conditions. *Nanomaterials* **2018**, *8*, 775. [CrossRef]
9. Mukhopadhyay, S.; Das, A.; Jana, T.; Das, S.K. Fabricating a MOF Material with Polybenzimidazole into an Efficient Proton Exchange Membrane. *ACS Appl. Energy Mater.* **2020**, *3*, 7964–7977. [CrossRef]

10. Hu, L.; Gao, L.; Di, M.; Jiang, X.; Wu, X.; Yan, X.; Li, X.; He, G. Ion/Molecule-selective transport nanochannels of membranes for redox flow batteries. *Energy Storage Mater.* **2021**, *34*, 648–668. [[CrossRef](#)]
11. Peng, S.; Wu, X.; Yan, X.; Gao, L.; Zhu, Y.; Zhang, D.; Li, J.; Wang, Q.; He, G. Polybenzimidazole membranes with nanophase-separated structure induced by non-ionic hydrophilic side chains for vanadium flow batteries. *J. Mater. Chem. A* **2018**, *6*, 3895–3905. [[CrossRef](#)]
12. Aberoumand, S.; Woodfield, P.; Shabani, B.; Dao, D.V. Advances in electrode and electrolyte improvements in vanadium redox flow batteries with a focus on the nanofluidic electrolyte approach. *Phys. Rep.* **2020**, *881*, 1–49. [[CrossRef](#)]
13. Lou, J.; You, D.; Li, X. Step-by-Step Modification of Graphite Felt Electrode for Vanadium Redox Flow Battery. *J. Electrochem.* **2020**, *26*, 876–884.
14. Jirabovornwisut, T.; Arpornwichanop, A. A review on the electrolyte imbalance in vanadium redox flow batteries. *Int. J. Hydrogen Energy* **2019**, *44*, 24485–24509. [[CrossRef](#)]
15. Khataee, A.; Nederstedt, H.; Jannasch, P.; Lindström, R.W. Poly(arylene alkylene)s functionalized with perfluorosulfonic acid groups as proton exchange membranes for vanadium redox flow batteries. *J. Membr. Sci.* **2023**, *671*, 121390. [[CrossRef](#)]
16. Tempelman, C.H.L.; Jacobs, J.F.; Balzer, R.M.; Degirmenci, V. Membranes for all vanadium redox flow batteries. *J. Energy Storage* **2020**, *32*, 101754. [[CrossRef](#)]
17. Yang, S.; Ahn, Y.; Kim, D. Poly(arylene ether ketone) proton exchange membranes grafted with long aliphatic pendant sulfonated groups for vanadium redox flow batteries. *J. Mater. Chem. A* **2017**, *5*, 2261–2270. [[CrossRef](#)]
18. Gubler, L. Membranes and separators for redox flow batteries. *Curr. Opin. Electrochem.* **2019**, *18*, 31–36. [[CrossRef](#)]
19. Zhang, L.; Ling, L.; Xiao, M.; Han, D.; Wang, S.; Meng, Y. Effectively suppressing vanadium permeation in vanadium redox flow battery application with modified Nafion membrane with nacre-like nanoarchitectures. *J. Power Sources* **2017**, *352*, 111–117. [[CrossRef](#)]
20. Lee, W.; Konovalova, A.; Tsoy, E.; Park, G.; Henkensmeier, D.; Kwon, Y. Alkaline naphthoquinone-based redox flow batteries with a crosslinked sulfonated polyphenylsulfone membrane. *Int. J. Energy Res.* **2022**, *46*, 12988–13002. [[CrossRef](#)]
21. Liu, S.; Sang, X.; Wang, L.; Zhang, J.; Song, J.; Han, B. Incorporation of metal-organic framework in polymer membrane enhances vanadium flow battery performance. *Electrochim. Acta* **2017**, *257*, 243–249. [[CrossRef](#)]
22. Zhou, X.; Zhao, T.; An, L.; Wei, L.; Zhang, C. The use of polybenzimidazole membranes in vanadium redox flow batteries leading to increased coulombic efficiency and cycling performance. *Electrochim. Acta* **2015**, *153*, 492–498. [[CrossRef](#)]
23. Ren, X.; Zhao, L.; Che, X.; Cai, Y.; Li, Y.; Li, H.; Chen, H.; He, H.; Liu, J.; Yang, J. Quaternary ammonium groups grafted polybenzimidazole membranes for vanadium redox flow battery applications. *J. Power Sources* **2020**, *457*, 228037. [[CrossRef](#)]
24. Wang, Y.; Feng, K.; Ding, L.; Wang, L.; Han, X. Influence of solvent on ion conductivity of polybenzimidazole proton exchange membranes for vanadium redox flow batteries. *Chin. J. Chem. Eng.* **2020**, *28*, 1701–1708. [[CrossRef](#)]
25. Lee, W.; Kwon, B.W.; Jung, M.; Serhiichuk, D.; Henkensmeier, D.; Kwon, Y. Iron-vanadium redox flow batteries with polybenzimidazole membranes: High coulomb efficiency and low capacity loss. *J. Power Sources* **2019**, *439*, 227079. [[CrossRef](#)]
26. Noh, C.; Serhiichuk, D.; Malikh, N.; Kwon, Y.; Henkensmeier, D. Optimizing the performance of meta-polybenzimidazole membranes in vanadium redox flow batteries by adding an alkaline pre-swelling step. *Chem. Eng. J.* **2021**, *407*, 126574. [[CrossRef](#)]
27. Wang, L.; Pingitore, A.T.; Xie, W.; Yang, Z.; Perry, M.L.; Benicewicz, B.C. Sulfonated PBI Gel Membranes for Redox Flow Batteries. *J. Electrochem. Soc.* **2019**, *166*, A1449–A1455. [[CrossRef](#)]
28. Jang, J.-K.; Kim, T.-H.; Yoon, S.J.; Lee, J.Y.; Lee, J.-C.; Hong, Y.T. Highly proton conductive, dense polybenzimidazole membranes with low permeability to vanadium and enhanced H<sub>2</sub>SO<sub>4</sub> absorption capability for use in vanadium redox flow batteries. *J. Mater. Chem. A* **2016**, *4*, 14342–14355. [[CrossRef](#)]
29. Noh, C.; Jung, M.; Henkensmeier, D.; Nam, S.W.; Kwon, Y. Vanadium Redox Flow Batteries Using meta-Polybenzimidazole-Based Membranes of Different Thicknesses. *ACS Appl. Mater. Interfaces* **2017**, *9*, 36799–36809. [[CrossRef](#)]
30. Peng, S.; Yan, X.; Zhang, D.; Wu, X.; Luo, Y.; He, G. A H<sub>3</sub>PO<sub>4</sub> preswelling strategy to enhance the proton conductivity of a H<sub>2</sub>SO<sub>4</sub>-doped polybenzimidazole membrane for vanadium flow batteries. *RSC Adv.* **2016**, *6*, 23479–23488. [[CrossRef](#)]
31. Pang, B.; Wu, X.; Guo, Y.; Yang, M.; Du, R.; Chen, W.; Yan, X.; Cui, F.; He, G. Anionic conductive group tunable amphoteric polybenzimidazole ion conductive membrane for vanadium redox flow battery. *J. Membr. Sci.* **2023**, *670*, 121351. [[CrossRef](#)]
32. Chen, Y.; Xiong, P.; Xiao, S.; Zhu, Y.; Peng, S.; He, G. Ion conductive mechanisms and redox flow battery applications of polybenzimidazole-based membranes. *Energy Storage Mater.* **2022**, *45*, 595–617. [[CrossRef](#)]
33. Do, X.H.; Abbas, S.; Ikhsan, M.M.; Choi, S.; Ha, H.Y.; Azizi, K.; Hjuler, H.A.; Henkensmeier, D. Membrane Assemblies with Soft Protective Layers: Dense and Gel-Type Polybenzimidazole Membranes and Their Use in Vanadium Redox Flow Batteries. *Small* **2022**, *18*, 2206284. [[CrossRef](#)] [[PubMed](#)]
34. Ding, L.; Song, X.; Wang, L.; Zhao, Z. Enhancing proton conductivity of polybenzimidazole membranes by introducing sulfonate for vanadium redox flow batteries applications. *J. Membr. Sci.* **2019**, *578*, 126–135. [[CrossRef](#)]
35. Du, Y.; Gao, L.; Hu, L.; Di, M.; Yan, X.; An, B.; He, G. The synergistic effect of protonated imidazole-hydroxyl-quaternary ammonium on improving performances of anion exchange membrane assembled flow batteries. *J. Membr. Sci.* **2020**, *603*, 118011. [[CrossRef](#)]
36. Song, X.; Ding, L.; Wang, L.; He, M.; Han, X. Polybenzimidazole membranes embedded with ionic liquids for use in high proton selectivity vanadium redox flow batteries. *Electrochim. Acta* **2019**, *295*, 1034–1043. [[CrossRef](#)]

37. Yang, P.; Long, J.; Xuan, S.; Wang, Y.; Zhang, Y.; Li, J.; Zhang, H. Branched sulfonated polyimide membrane with ionic cross-linking for vanadium redox flow battery application. *J. Power Sources* **2019**, *438*, 226993. [[CrossRef](#)]
38. Ahn, Y.; Kim, D. Ultra-low vanadium ion permeable electrolyte membrane for vanadium redox flow battery by pore filling of PTFE substrate. *Energy Storage Mater.* **2020**, *31*, 105–114. [[CrossRef](#)]
39. Liang, D.; Wang, S.; Ma, W.; Wang, D.; Liu, G.; Liu, F.; Cui, Y.; Wang, X.; Yong, Z.; Wang, Z. A low vanadium permeability sulfonated polybenzimidazole membrane with a metal-organic framework for vanadium redox flow batteries. *Electrochim. Acta* **2022**, *405*, 139795. [[CrossRef](#)]
40. Luo, T.; David, O.; Gendel, Y.; Wessling, M. Porous poly(benzimidazole) membrane for all vanadium redox flow battery. *J. Power Sources* **2016**, *312*, 45–54. [[CrossRef](#)]
41. Yan, X.; Dong, Z.; Di, M.; Hu, L.; Zhang, C.; Pan, Y.; Zhang, N.; Jiang, X.; Wu, X.; Wang, J.; et al. A highly proton-conductive and vanadium-rejected long-side-chain sulfonated polybenzimidazole membrane for redox flow battery. *J. Membr. Sci.* **2020**, *596*, 117616. [[CrossRef](#)]
42. Wang, D.; Wang, S.; Tian, X.; Li, J.; Liu, F.; Wang, X.; Chen, H.; Mao, T.; Liu, G. Ethyl phosphoric acid grafted amino-modified polybenzimidazole with improved long-term stability for high-temperature proton exchange membrane applications. *Int. J. Hydrogen Energy* **2020**, *45*, 3176–3185. [[CrossRef](#)]
43. Liu, F.; Wang, S.; Wang, D.; Liu, G.; Cui, Y.; Liang, D.; Wang, X.; Yong, Z.; Wang, Z. Multifunctional polymeric ionic liquids cross-linked polybenzimidazole membrane with excellent long-term stability for high temperature-proton exchange membranes fuel cells. *J. Power Sources* **2021**, *494*, 229732. [[CrossRef](#)]
44. Chen, H.; Wang, S.; Li, J.; Liu, F.; Tian, X.; Wang, X.; Mao, T.; Xu, J.; Wang, Z. Novel cross-linked membranes based on polybenzimidazole and polymeric ionic liquid with improved proton conductivity for HT-PEMFC applications. *J. Taiwan Inst. Chem. Eng.* **2019**, *95*, 185–194. [[CrossRef](#)]
45. Cui, Y.; Wang, S.; Wang, D.; Liu, G.; Liu, F.; Liang, D.; Wang, X.; Yong, Z.; Wang, Z. HT-PEMs based on carbazole grafted polybenzimidazole with high proton conductivity and excellent tolerance of phosphoric acid. *J. Membr. Sci.* **2021**, *637*, 119610. [[CrossRef](#)]
46. Peng, S.; Yan, X.; Wu, X.; Zhang, D.; Luo, Y.; Su, L.; He, G. Thin skinned asymmetric polybenzimidazole membranes with readily tunable morphologies for high-performance vanadium flow batteries. *RSC Adv.* **2017**, *7*, 1852–1862. [[CrossRef](#)]
47. Sizov, V.E.; Kondratenko, M.S.; Gallyamov, M.O.; Stevenson, K.J. Advanced porous polybenzimidazole membranes for vanadium redox batteries synthesized via a supercritical phase-inversion method. *J. Supercrit. Fluids* **2018**, *137*, 111–117. [[CrossRef](#)]
48. Che, X.; Zhao, H.; Ren, X.; Zhang, D.; Wei, H.; Liu, J.; Zhang, X.; Yang, J. Porous polybenzimidazole membranes with high ion selectivity for the vanadium redox flow battery. *J. Membr. Sci.* **2020**, *611*, 118359. [[CrossRef](#)]
49. Mu, T.; Tang, W.; Jin, Y.; Che, X.; Liu, J.; Yang, J. Ether-Free Poly(*p*-terphenyl-*co*-acetylpyridine) Membranes with Different Thicknesses for Vanadium Redox Flow Batteries. *ACS Appl. Energy Mater.* **2022**, *5*, 11713–11722. [[CrossRef](#)]

**Disclaimer/Publisher's Note:** The statements, opinions and data contained in all publications are solely those of the individual author(s) and contributor(s) and not of MDPI and/or the editor(s). MDPI and/or the editor(s) disclaim responsibility for any injury to people or property resulting from any ideas, methods, instructions or products referred to in the content.